# PROOF COVER SHEET

Author(s): Jahrule Alam
Article title: A multiscale eddy simulation methodology for the atmospheric Ekman boundary layer
Article no: GGAF 975127
Enclosures: 1) Query sheet
2) Article proofs

Dear Author,

**1. Please check these proofs carefully.** It is the responsibility of the corresponding author to check these and approve or amend them. A second proof is not normally provided. Taylor & Francis cannot be held responsible for uncorrected errors, even if introduced during the production process. Once your corrections have been added to the article, it will be considered ready for publication.

Please limit changes at this stage to the correction of errors. You should not make trivial changes, improve prose style, add new material, or delete existing material at this stage. You may be charged if your corrections are excessive (we would not expect corrections to exceed 30 changes).

For detailed guidance on how to check your proofs, please paste this address into a new browser window: http://journalauthors.tandf.co.uk/production/checkingproofs.asp

Your PDF proof file has been enabled so that you can comment on the proof directly using Adobe Acrobat. If you wish to do this, please save the file to your hard disk first. For further information on marking corrections using Acrobat, please paste this address into a new browser window: http://journalauthors.tandf.co.uk/production/acrobat.asp

**2. Please review the table of contributors below and confirm that the first and last names are structured correctly and that the authors are listed in the correct order of contribution.** This check is to ensure that your name will appear correctly online and when the article is indexed.

| Sequence | Prefix | Given name(s) | Surname | Suffix |
|---|---|---|---|---|
| 1 | | Jahrul | Alam | |
| 2 | | Mo Rokibul | Islam | |

Queries are marked in the margins of the proofs, and you can also click the hyperlinks below.

# AUTHOR QUERIES

**General points**:

1. **Permissions:** You have warranted that you have secured the necessary written permission from the appropriate copyright owner for the reproduction of any text, illustration, or other material in your article. Please see http://journalauthors.tandf.co.uk/permissions/usingThirdPartyMaterial.asp.
2. **Third-party content:** If there is third-party content in your article, please check that the rightsholder details for re-use are shown correctly.
3. **Affiliation:** The corresponding author is responsible for ensuring that address and email details are correct for all the co-authors. Affiliations given in the article should be the affiliation at the time the research was conducted. Please see http://journalauthors.tandf.co.uk/preparation/writing.asp.
4. **Funding:** Was your research for this article funded by a funding agency? If so, please insert 'This work was supported by <insert the name of the funding agency in full>', followed by the grant number in square brackets '[grant number xxxx]'.
5. **Supplemental data and underlying research materials:** Do you wish to include the location of the underlying research materials (e.g. data, samples or models) for your article? If so, please insert this sentence before the reference section: 'The underlying research materials for this article can be accessed at <full link>/ description of location [author to complete]'. If your article includes supplemental data, the link will also be provided in this paragraph. See <http://journalauthors.tandf.co.uk/preparation/multimedia.asp> for further explanation of supplemental data and underlying research materials.
6. The **CrossRef database** (www.crossref.org/) has been used to validate the references. Mismatches will have resulted in a query.

| | |
|---|---|
| AQ1 | There is a mismatch between the history dates on your accepted manuscript and the information automatically logged by the online submission system. We have followed the dates in the manuscript; please check and confirm that this is correct. |
| AQ2 | Please provide missing page numbers for the 'Alam (2011)' references list entry. |
| AQ3 | Please provide missing last page number for the 'Brasseur and Wei (2010)' references list entry. |
| AQ4 | Please provide missing city for the 'Garratt (1992)' references list entry. |

| | |
|---|---|
| AQ5 | Please provide missing volume number and page numbers for the ‘Hatlee and Wyngaard (2007)’ references list entry. |
| AQ6 | Please provide missing volume number for the ‘Nordbo and Katul (2012)’ references list entry. |
| AQ7 | Please provide missing city for the ‘Pielke (2002)’ references list entry. |

**How to make corrections to your proofs using Adobe Acrobat/Reader**

Taylor & Francis offers you a choice of options to help you make corrections to your proofs. Your PDF proof file has been enabled so that you can edit the proof directly using Adobe Acrobat/Reader. This is the simplest and best way for you to ensure that your corrections will be incorporated. If you wish to do this, please follow these instructions:

1. Save the file to your hard disk.
2. Check which version of Adobe Acrobat/Reader you have on your computer. You can do this by clicking on the "Help" tab, and then "About".

   If Adobe Reader is not installed, you can get the latest version free from http://get.adobe.com/reader/.
3. If you have Adobe Acrobat/Reader 10 or a later version, click on the "Comment" link at the right-hand side to view the Comments pane.
4. You can then select any text and mark it up for deletion or replacement, or insert new text as needed. Please note that these will clearly be displayed in the Comments pane and secondary annotation is not needed to draw attention to your corrections. If you need to include new sections of text, it is also possible to add a comment to the proofs. To do this, use the Sticky Note tool in the task bar. Please also see our FAQs here: http://journalauthors.tandf.co.uk/production/index.asp.
5. Make sure that you save the file when you close the document before uploading it to CATS using the "Upload File" button on the online correction form. If you have more than one file, please zip them together and then upload the zip file.

   If you prefer, you can make your corrections using the CATS online correction form.

**Troubleshooting**

**Acrobat help:** http://helpx.adobe.com/acrobat.html
**Reader help:** http://helpx.adobe.com/reader.html

Please note that full user guides for earlier versions of these programs are available from the Adobe Help pages by clicking on the link "Previous versions" under the "Help and tutorials" heading from the relevant link above. Commenting functionality is available from Adobe Reader 8.0 onwards and from Adobe Acrobat 7.0 onwards.

**Firefox users:** Firefox's inbuilt PDF Viewer is set to the default; please see the following for instructions on how to use this and download the PDF to your hard drive:
http://support.mozilla.org/en-US/kb/view-pdf-files-firefox-without-downloading-them#w_using-a-pdf-reader-plugin

GGAF 975127
28-10-2014
Revision
CE:YS QA:MG

*Geophysical and Astrophysical Fluid Dynamics*, 2014
http://dx.doi.org/10.1080/03091929.2014.975127

Taylor & Francis
Taylor & Francis Group

# A multiscale eddy simulation methodology for the atmospheric Ekman boundary layer

JAHRUL ALAM* and MO ROKIBUL ISLAM[1]

AQ1 Department of Mathematics and Statistics, Memorial University of Newfoundland, St John's, Newfoundland A1C 5S7, Canada

(*Received 20 February 2013; in final form 24 September 2014*)

In a large eddy simulation (LES), resolving the wide spectrum of large turbulent eddies from O(m) to O(km) in the atmospheric boundary layer (ABL) requires $O(10^9)$ computational degrees of freedom; however, these eddies are intermittent in space and time. In this research, we take advantage of the spatial intermittency in a neutrally stratified atmospheric Ekman boundary layer, and study the development of a novel LES methodology. Using the second generation wavelet transform, the proposed model filters the large eddies into distinct groups of significant and insignificant eddies. We show that the significant eddies are sufficient to resolve the physics of the flow. The effects of insignificant eddies are modelled with the proposed multiscale parameterization scheme. The results of the proposed model have been found to be in good agreement with that of an equivalent reference model, experimental data, and asymptotic boundary layer theory. We have found that the number of significant eddies in a neutrally stratified ABL is much lower than the number of resolved eddies in a reference model. The overall algorithm is asymptotically optimal – the CPU time is approximately proportional to the number of resolved eddies. The proposed methodology suggests a potentially novel research direction that may be employed to address a number of computational challenges that must be faced in the field of atmospheric modeling.

*Keywords:* Large eddy simulation; Multiscale modeling; Wavelet; Ekman boundary layer; Atmospheric modeling

## 1. Introduction

The Atmospheric Boundary Layer (ABL) is characterized by complex multiscale phenomena involving intermittent turbulence. A popular computational approach for the ABL is the large eddy simulation (LES) methodology, which is based on the pioneering works of Smagorinsky (1963) and Deardorff (1970) (see, e.g. Deardorff 1972, Moeng 1984, Mason and Thomson 1987, Andrén *et al.* 1994, Zhou and Chow 2011). In LES, it is assumed that most of the transport of momentum and scalars can be directly resolved via numerical solution of spatially averaged Navier–Stokes equations, and the dynamics of small eddies can be predicted with a subgrid-scale (SGS) model, provided that a major fraction of energetic scales is resolved. In practice, inaccuracies persist in the LES prediction of the dynamics of small

*Corresponding author. Email: alamj@mun.ca
[1]Present address: Department of Atmospheric and Oceanic Sciences, McGill University, Quebec H3A 0B9, Canada.

eddies that occur near the atmospheric surface layer (Senocak *et al.* 2007). In order to predict the near-surface transport mechanisms accurately, LES must employ a very fine grid (about 1m for $\Delta_{\text{LES}}$) (Brasseur and Wei 2010, Sullivan and Patton 2011); otherwise, near-surface models must be used to supplement SGS models (Hatlee and Wyngaard 2007, Senocak *et al.* 2007). To resolve small eddies without any *ad hoc* parameterization, a direct numerical simulation (DNS) model was developed and validated for studying rotating turbulence in both neutral and buoyant Ekman boundary layers (Coleman *et al.* 1990, 1992, 1994, Coleman 1999), and there is a growing interest in such DNS modelling (Shingai and Kawamura 2004, Miyashita *et al.* 2006, Morris *et al.* 2010, Scott *et al.* 2010, Marlatt *et al.* 2012). Although simulations with both LES and DNS have confirmed that the most important physics of the ABL flow are intermittent over multiple length and time scales (e.g. Basu and Porté-Agel 2006, Vindel and Yagüe 2011), existing LES or DNS models do not fully exploit the multiscale and intermittent nature of turbulent Ekman flow.

In general, the ABL is turbulent and spatially intermittent (Wyngaard 1992). However, during very stable conditions, the nighttime ABL is often characterized by brief *episodes* of turbulent "bursts" (Schubert 1977, Nai-Ping *et al.* 1983, Coulter 1990) – a phenomenon that has been called global intermittency (see e.g. figure 1 of Costa *et al.* 2011), where the interaction between turbulence and buoyancy appears as a sequence of turbulent and calm periods (Sorbjan 2006, Zhou and Chow 2012). Intermittency is a challenge to the field of computational atmospheric modeling because during a calm period, when turbulence is suppressed, a low resolution in both space and time may be adequate to resolve the flow. In contrast, during a turbulent period, an extremely high resolution is needed to resolve many of the small-scale eddies. Since the important physics is intermittent, and confined into a fraction of the boundary layer (e.g. Townsend 1948, Batchelor and Townsend 1949), a multiscale model could refine and coarsen the mesh locally only where it is necessary – as well as – adjust the time step. This approach helps to address the gap between the large scale physics and small-scale phenomena in such a complex and multiscale flow as in the ABL. For this reason, dynamically adaptive mesh refinement (AMR) models are being developed for resolving non-hydrostatic phenomena in mesoscale atmospheric models (Skamarock *et al.* 1989, Jablonowski *et al.* 2006, Skamarock *et al.* 2012).

The present article examines a multiscale eddy simulation (MES) model for the neutrally stratified atmospheric Ekman boundary layer. This article assumes eddy as an elementary swirling structure, which is associated with a position, a length scale, and a strength. In order to model intermittent flow in the ABL, we propose to categorize resolved eddies into a group of significant eddies with different length scales, which govern the most important physics of the flow. The remaining eddies belong to the group of insignificant eddies. Each eddy is associated with a position, a scale, and a strength. We call an eddy significant with respect to a threshold $\epsilon$ if all components of its 3D velocity have wavelet coefficients larger than $\epsilon$. We employ the second-generation interpolating wavelet transform using the lifting scheme with $O(\mathcal{N})$ operations (Sweldens 1997), where $\mathcal{N}$ is the number of resolved eddies. Using the lifting wavelet transform (Sweldens 1997, Alam 2011), we can extract the position, scale, and strength of an eddy. The significant eddies are resolved, and the insignificant eddies are parameterized, where we have investigated and developed a multiscale parameterization scheme for unresolved motion, as well as a fast multiscale solution algorithm. The position of the significant intermittent eddies compose an adaptive mesh, which is an advantage of the present approach. In other words, the present model adapts the mesh dynamically to the physics of the significant fraction of a flow. In contrast, an AMR model adapts the mesh according to an *ad hoc* error estimation criterion (see Berger and Collela 1989, Skamarock *et al.* 1989).

For the purpose of reference in what follows, we will denote the present development a MES model throughout the remainder of this article. The model is outlined in section 2, and validated in section 3. Section 4 summarizes the present results and discusses potential future developments.

## 2. The MES methodology

### 2.1. *A wavelet approach to model spatial intermittency*

The promise of wavelets for modeling homogeneous isotropic turbulence (Farge *et al.* 1999, Goldstein and Vasilyev 2004, Kevlahan *et al.* 2007, Schneider and Vasilyev 2010), and for less idealized applications within LES (de la Llave Plata and Cant 2010, Stefano and Vasilyev 2013) has been studied previously. In the atmospheric science community, wavelets are often used as a powerful tool for statistical analysis of atmospheric data (e.g. Domingues *et al.* 2005, Nordbo and Katul 2013). Alam (2011) developed a wavelet-based multiscale model for thermally driven non-hydrostatic circulations in the dry atmosphere. The work of Farge *et al.* (1999) demonstrates decomposition of a turbulent flow into multiple length scales, whereas the present article employs wavelets to model spatial intermittency in the ABL.

In a classical LES, turbulent motions (eddies) are resolved using $N$ grid points (or wavenumbers) per domain size in a given dimension, whereas only a fraction of the calculations (grid volumes) are actually required to capture the important dynamics of an intermittent flow at a desired scale (e.g. Frisch *et al.* 1978). In the atmospheric Ekman boundary layer, the intermittency of the near-surface eddies is strongly affected by a secondary circulation induced by surface drag, while the turbulent flow is continuously forced by the geostrophic wind and the Earth's rotation. Note that for neutral conditions, shear production of turbulent kinetic energy is much stronger than buoyant production. In order to visualize how a classical LES would be limited in resolving the space-time intermittency of this secondary circulation, it

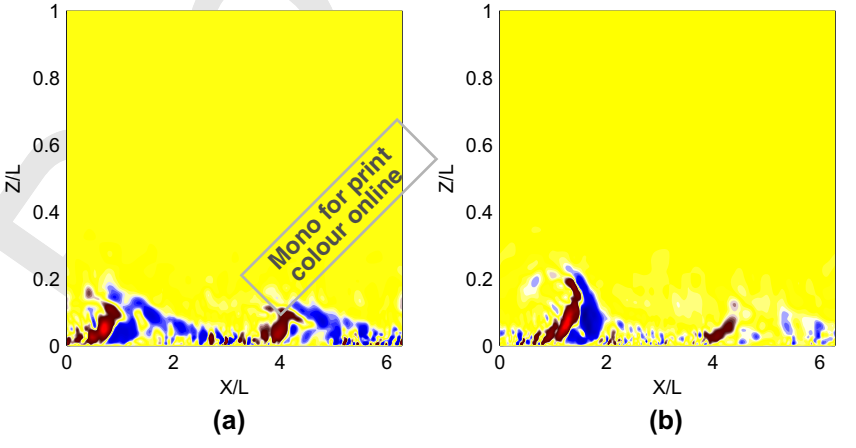


Figure 1. A vertical cross-section of the $y$-component vorticity is presented to visualize intermittency of turbulent eddies in a neutrally stratified ABL. The Reynolds number for this simulation is 16 000 which is based on a geostrophic wind of 8m/s, model height of $L = 4$km, and an eddy viscosity of $2\text{m}^2/\text{s}$ (see table 1). Note significant counter-clockwise, clockwise eddies with respect to the $y$-axis, and less-significant eddies are represented with red, blue, and yellow, respectively. (a) and (b) are simulations at 10 and 11.2 h, respectively, from the model initialization.

is convenient to present snapshots from our MES simulations of a neutral ABL. Given the details of the simulation and parameters in section 3, figure 1 presents two instances of the ABL in a fixed vertical cross section along the direction of geostrophic wind. Here, a principal observation is that turbulence in the lowest 1km of the ABL is intermittent in space and time. The intermittency of energetic scales is apparent as the surface is approached, where isolated bursts are accompanied by relatively quiescent regions. Clearly, a fine resolution is required for resolving a necessary fraction of the energetic scales. With a given SGS model, the resolution ($\Delta_{\text{LES}}$) for capturing a necessary fraction of the energetic scales of the turbulent flow in figure 1(a) may not capture an equivalent fraction of the same in figure 1(b) because bursts in vorticity at $t = 11.2$ h are confined into smaller scales with respect to that at $t = 10$ h, and this space-time intermittency is an unresolved challenge for classical LES models.

Studies have indicated that this near-surface intermittency requires either the refinement of the LES grid and/or the development of application-specific near surface models (Senocak *et al.* 2007, Brasseur and Wei 2010). In this article, we study how to utilize the wavelet method on the development of a multiscale numerical modelling approach, and its verification for such space-time intermittency in the Ekman boundary layer.

### 2.2. *Intermittency and multiscale decomposition*

In this section, we present the methodology needed to separate significant and insignificant eddies, and define the associated nomenclature. Note that the term "eddy" is a loose concept used to represent the scales of a turbulent motion.

Let $\Delta$ represent the integral length scale, and $\Delta_s = 2^{-s}\Delta$ be the length scale of the resolved eddies for a simulation at the refinement level $s$. In other words, $\Delta_{\text{LES}} = \Delta_s$, if a classical LES is employed. The entire volume $\Delta^3$ is occupied by $N = (\Delta/\Delta_s)^3$ uniformly distributed eddies. Suppose that we have a process to measure the strength of an eddy. As studied by Frisch *et al.* (1978), in the inertial range of turbulence only $\mathcal{N}$ eddies, having length scales in the range between $\Delta_s$ and $\Delta$, will have a strength that is greater than a threshold $\epsilon$, where $\mathcal{N} \ll N$. Each time an eddy breaks down, it loses strength. In other words, all eddies with a strength $< \epsilon$ will have a scale $< \Delta_s$. We can filter out $\mathcal{N}$ significant eddies based on a threshold ($\epsilon$) of their strength. If we fix $\epsilon$, the smallest scale $\Delta_s$ of resolved $\mathcal{N}$ eddies, i.e. the final refinement level $s$, may depend on the particular turbulent flow that is being simulated, and can be obtained dynamically. In contrast to classical LES, $\Delta_s$ is not prescribed, but the threshold $\epsilon$ determines $\Delta_s$. During a time step, if turbulence is suppressed or enhanced, the number of eddies will be adapted to exploit the intermittency. Furthermore, the above process is a low-pass filter of significant eddies because all discarded eddies with a strength $< \epsilon$ are associated with dimensionless wavenumbers up to $2^s$. Clearly, $\Delta_s$ may decrease and $\mathcal{N}$ may increase if we reduce $\epsilon$. In other words, both the resolved frequency and the CPU time will be controlled with *a priori* turbulence threshold $\epsilon$. In the present work, we employ a second-generation wavelet decomposition of the velocity field to model $\mathcal{N}$ significant eddies, and estimate the strength of an eddy based on the magnitude of the corresponding wavelet coefficient. We estimate $\mathcal{N} \sim \epsilon^{-3/p}$ for the number of significant eddies, where $p$ denotes the number of vanishing moments of the wavelet system (Alam 2006).

We associate the physical position of each eddy in the 3-dimensional space to a grid point (i.e. node), which is represented by an index $k$. The same symbol ($k$) can also be retained, for simplicity, when we illustrate the method in 1-dimension. Let $\langle u_i \rangle_k^s$ denote the mean velocity of an eddy of size $\Delta_s$ (or scale $s$) and $\langle u_i \rangle^s$ denote the mean velocity associated with all eddies having characteristic dimensionless wavenumbers or frequencies $2^s$. For a fixed $s$, $\langle u_i \rangle^s$ is

the same as the mean velocity $\langle u_i \rangle$ in a classical LES. Let $\langle u_i \rangle_\epsilon^s$ be the filtered mean velocity associated with $\mathcal{N}$ significant eddies. The total velocity is given by

$$u_i = \langle u_i \rangle_\epsilon^s + u_i' , \tag{1}$$

where $u_i'$ denote the velocity of insignificant eddies and $i = 1, 2, 3$. Note that the filtering operator $\langle \cdot \rangle_\epsilon^s$ extracts corresponding information associated with eddies that have a strength $\geq \epsilon$. First, we need to decompose $u_i$ scale-by-scale to get $\langle u_i \rangle^s$. Then, we need to estimate the strength of eddies at each scale, and filter them to obtain $\langle u_i \rangle_\epsilon^s$. To do so, we will take a wavelet transform of sampled data $u_i$, discard all wavelet coefficients that have a magnitude less than $\epsilon$, and take the inverse wavelet transform.

Applying the following lifting scheme, we give minimal technical information for brevity, but intend that the proposed MES methodology may be implemented in an existing ABL code; hence, we do not discuss the theory of second-generation wavelets in this article (see Mallat 2008).

### 2.3. *The lifting scheme*

The intermittency of energetic scales (e.g. Frisch *et al.* 1978) is demonstrated schematically in figure 2(a). For simplicity, consider a 1-dimensional example in figure 2(b) with $2^s + 1$ eddies aligned in a straight line. In this example, for position index $k = 0, 1, \cdots, 2^s$, we denote the mean velocity of eddies at level $s + 1$ by $\langle u_i \rangle_{2k}^{s+1}$ and mark their position *red* (e.g. red positions at level 3 in figure 2(b) for $s = 2$). We organize another $2^s$ *black* eddies, having mean velocities $\langle u_i \rangle_{2k-1}^{s+1}$, in an alternating arrangement (i.e. red-black), resulting in a total of $2^{s+1} + 1$ eddies at level $s + 1$. For example, in figure 2(b), we have 4 black eddies and 5 red eddies at level 3. The red-black arrangement of eddies at level 4 is also presented. We can think that black eddies represent the leading order modes of the truncated part of the energy spectrum. Clearly, knowing the strength of black eddies, we can extract turbulent bursts as the

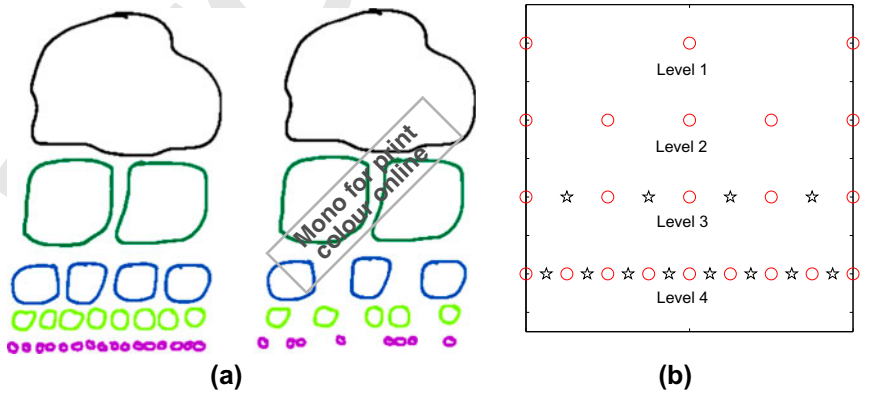


Figure 2. (a) A schematic demonstration of the energy cascade; eddies of the same scale have been marked with a color, using black for the largest scale. (Column 1) At each scale eddies are space filling; (Column 2) eddies are less and less space filling as the dissipative scale is approached. Note the eddies are in fact embedded within each other. (b) Positions and scales of intermittent eddies. This demonstration assumes level 1 and level 4 as integral and dissipative scales, respectively. For brevity, red-black positions are shown at level 3 and 4.

dissipative scale is approached. Our aim is twofold. First, using the lifting scheme (Sweldens 1997), we want to decompose the mean velocity $\langle u_i\rangle_k^{s+1}$ (for $k = 0, \cdots, 2^{s+1}$) into one group $\langle u_i\rangle_k^s$ for $k = 0, \cdots\cdots, 2^s$, representing information at level $s$ and another group $\langle d_i\rangle_k^s$ for $k = 1, \cdots\cdots, 2^s$, representing the missing details at level $s$. More specifically, we have

$$\langle u_i\rangle_k^s = \langle u_i\rangle_{2k}^{s+1} + \langle \tilde{u_i}\rangle_{2k}^{s+1}, \qquad k = 0, \cdots\cdots 2^s, \tag{2a}$$

$$2\langle d_i\rangle_k^s = \langle u_i\rangle_{2k-1}^{s+1} - \langle \tilde{u_i}\rangle_{2k-1}^{s+1}, \qquad k = 1, \cdots\cdots 2^s. \tag{2b}$$

Clearly (2a) leads to an upscaling of the velocity field from the finer scale $s+1$ to the coarser scale $s$. The downscaling is the inverse of (2a,b). In (2b), $\langle \tilde{u_i}\rangle_{2k-1}^{s+1}$ is an approximation or prediction of $\langle u_i\rangle_{2k-1}^{s+1}$ using mean velocities $\langle u_i\rangle_{2k}^{s+1}$ from some selected locations at level $s$. As a linear prediction, one would use two nodes such that $\langle \tilde{u_i}\rangle_{2k-1}^{s+1} = \frac{1}{2}[\langle u_i\rangle_{2k-2}^{s+1} + \langle u_i\rangle_{2k}^{s+1}]$, and an appropriate polynomial can be used for a higher order prediction. Similarly, $\langle \tilde{u_i}\rangle_{2k}^{s+1}$ are obtained based on computed $\langle d_i\rangle_k^s$ from (2b). As a result, all eddies at level $s+1$ are decomposed into one group at level $s$ *via* (2a) and another group representing the missing details at level $s$ *via* (2b). In the present development, we have used 6 nodes for interpolations in (2a,b), which results in 6th order lifted interpolating wavelets (Sweldens 1997, Alam 2011, Stefano and Vasilyev 2013).

Second, the wavelet decomposition has the following advantage in the context of the present MES. For a chosen $k$, if $\langle u_i\rangle_{2k-1}^{s+1}$ is the mean velocity of an energy containing significant eddy, this eddy is highly correlated to its neighbours, and the magnitude of $\langle d_i\rangle_k^s$ is large. Hence, if $\left|\langle d_i\rangle_k^s\right| \geq \epsilon$, the corresponding eddy is marked significant at scale $s+1$. The process is applied to (2a) recursively for levels $s, s-1, \cdots, 1$, and significant eddies are marked at each level. We can recover the original velocity with inverse operations from (2a,b). Further technical details of the lifting scheme are outlined in Sweldens (1997). In 3D, we apply the lifting scheme in each direction, and obtain the wavelet decomposition for the 3D field. For all results in this article, we have applied the same threshold on each velocity component.

The following procedure has been proposed in this research so that we do not need to employ the entire velocity field at the finest level of resolution for filtering significant eddies.

### 2.4. *Governing equations, domain, and boundary conditions*

Let us consider an $f$-plane approximation of the ABL in a domain $L_x \times L_y \times L_z$, where $z$ is the vertical coordinate, and define the operator $\mathcal{L}$ by

$$\mathcal{L}u_i = \frac{\partial u_i}{\partial t} + u_j\frac{\partial u_i}{\partial x_j} + \frac{\partial P}{\partial x_i} + 2\epsilon_{ijk}\Omega_j(u_k - G_k), \tag{3}$$

such that $\mathcal{L}u_i = 0$, where $G_k$ represents geostrophic wind (see Chapter 4, Pielke 2002 and Chapter 2, Garratt 1992). The following filtered equations

$$\frac{\partial\langle u_i\rangle_\epsilon^s}{\partial x_i} = 0, \tag{4a}$$

$$\frac{\partial\langle u_i\rangle_\epsilon^s}{\partial t} + \langle u_j\rangle_\epsilon^s\frac{\partial\langle u_i\rangle_\epsilon^s}{\partial x_j} + \frac{\partial P}{\partial x_i} + 2\epsilon_{ijk}\Omega_j(\langle u_k\rangle_\epsilon^s - G_k) = -\frac{\partial\tau_{ij}}{\partial x_j} \tag{4b}$$

are obtained, where

$$\tau_{ij} = \underbrace{\langle\langle u_i\rangle_\epsilon^s u_j'\rangle_\epsilon^s + \langle u_i'\langle u_j\rangle_\epsilon^s\rangle_\epsilon^s}_{\tau_{ij}^I} + \underbrace{\langle u_i'u_j'\rangle_\epsilon^s}_{\tau_{ij}'},$$

and we have used the symbol $P$ (without $\langle\cdot\rangle_\epsilon^s$) in the filtered equation (4b) to indicate that the pressure term in (4b) is associated with enforcing the filtered incompressibility constraint (4a) (Alam 2011, Stefano and Vasilyev 2013). Equations (4a,b) model a rotating turbulent flow that is associated with the most significant eddies at scale $s$, and constitute a multiscale dynamical core for a neutrally stratified atmospheric Ekman boundary layer.

### 2.5. *Large eddy simulation*

To recover the classical LES (e.g. Deardorff 1970, Moeng 1984), we may drop the subscript $\epsilon$ from (1):

$$u_i \;=\; \langle u_i\rangle^s \;+ u_i' \,,$$

which means that the LES filter is employed by the numerical grid at scale $s$. The Smagorinsky (1963) model for the daviatoric part $\tau_{ij}^{\text{smag}} = \tau_{ij} - (1/3)\tau_{kk}\delta_{ij}$ of the SGS stress

$$\tau_{ij} \;=\; \langle u_i u_j\rangle^s \;-\; \langle u_i\rangle^s \langle u_j\rangle^s$$

is modeled by

$$\tau_{ij}^{\text{smag}} \;=\; -\,\nu S_{ij},$$

where

$$S_{ij} \;=\; \frac{1}{2}\left(\frac{\partial_j\langle u_i\rangle^s}{\partial x_i} \;+\; \frac{\partial_i\langle u_j\rangle^s}{\partial x_j}\right) \qquad \text{and} \qquad \nu \;=\; 2(C_s\Delta_{\text{LES}})^2\sqrt{2S_{ij}S_{ij}}\,.$$

The Smagorinsky constant $C_s$ may be adjusted (for example, Senocak *et al.* 2007 used $C_s = 0.18$). Typically, the filtered scale is defined by $\Delta_{\text{LES}} = (\Delta_x\cdot\Delta_y\cdot\Delta_z)^{1/3}$. The search for the best parameterization of the SGS is an open problem in LES research.

### 2.6. *Multiscale parameterization of insignificant eddies*

In the present MES, two components of the SGS stress $\tau_{ij}$ (i.e. $\tau_{ij}'$, $\tau_{ij}^I$ in (4b)) have been parameterized. The Reynolds stress $\tau_{ij}'$ can be modeled with a classical Smagorinsky (1963) treatment. For the purpose of comparison with the reference model, an eddy viscosity scheme has been used for $\tau_{ij}'$. We propose the following multiscale approach for parameterizing the stress $\tau_{ij}^I$. First, we estimate $\langle u_i\rangle_\epsilon^s$ from (4a,b) by replacing $\tau_{ij}$ with $\tau_{ij}'$ in (4b) (see section 2.7). Second, we incorporate the effect of $\tau_{ij}^I$ based upon an upscaled estimate $\langle u_i\rangle_\epsilon^{s-1}$ from (6a,b). This is done by obtaining an upscaling representation of the quantity

$$\frac{\partial\tau_{ij}^I}{\partial x_j} \;=\; -\,\frac{\partial\tau_{ij}'}{\partial x_j} - \mathcal{L}\langle u_i\rangle_\epsilon^s \,, \tag{5}$$

using the wavelet method (e.g. the last term in (6b)), and solving the following upscaling equations

$$\frac{\partial\langle u_i\rangle_\epsilon^{s-1}}{\partial x_i} = 0, \tag{6a}$$

$$\mathcal{L}\langle u_i\rangle_\epsilon^{s-1} = \mathcal{L}\langle\langle u_i\rangle_\epsilon^s\rangle_\epsilon^{s-1} + \left\langle\frac{\partial\tau_{ij}^I}{\partial x_j}\right\rangle_\epsilon^{s-1} \tag{6b}$$

for $\langle u_i \rangle_\epsilon^{s-1}$. Note that the interaction between eddies at scale $s$ with those at scale $s-1$ has been exploited on the right-hand side of (6b), where the first term employs $\tau'_{ij}$ and the second term – computed from (5) – employs $\tau^I_{ij}$. Therefore, estimating the large scale field $\langle u_i \rangle_\epsilon^{s-1}$ from (6b) and obtaining its downscaling estimate with inverse operations of (2a,b) to the smaller scale $s$ results in a computed flow $\langle u_i \rangle_\epsilon^{s}$ that incorporates the influence of both components of the stress $\tau^I_{ij}$ and $\tau'_{ij}$.

The solution procedure is based upon a recursive approach in which the flow computed from (6a,b) is upscaled until a desired large scale is reached, where turbulent eddies are not spatially intermittent. As soon as the large scale flow is computed, a recursive downscaling is employed until the smallest scale is reached. We refer to (4a,b) as the fine scale MES equations and (6a,b) as the large scale MES equations.

### 2.7. *Numerical procedure*

An important feature of the present MES model is the following. First, approximate solutions of the fine scale equations (4a,b) are used to form the coarse scale equations (6a,b). Next, approximate solutions of (6a,b) are used to predict the missing details between the two scales, which is used to improve the fine scale solution. The process is recursive, which means that on each scale, the solution is complemented by the missing details with respect to the coarser scale solution.

Since an adaptive wavelet methodology for turbulence exists (e.g. Farge *et al.* 1999, Alam 2006), this approach may also be used to solve the classical LES equations for ABL turbulence. However, the novelty of the present approach lies in what follows from the above multiscale approach, where two sets of MES equations are solved in contrast to one set of LES equations plus SGS parameterization.

The same numerical scheme has been applied to solve the fine scale equations (4a,b) and the large scale equations (6a,b). The overall numerical procedure is an extension of the method that was developed in Alam (2011), where methods for approximating spatial derivatives and implementing boundary conditions are briefly outlined (see also Alam 2006). It is important to note that the proposed MES methodology is not strictly dependent on the spatial discretization adopted in the present work, and can also be extended along with an existing ABL code.

In the present work, a fully implicit second order Crank–Nicolson method is used for both linear and nonlinear terms in (4b) and (6b), where a large system of the fully nonlinear equations are solved at each time step. This removes any restriction on the time step due to the nonlinear advection term. The maximum value of the Courant–Friedrichs–Lewy (CFL) number is 4 for all simulations presented in this article. On each scale, the discrete nonlinear system is approximated only with 3–5 iterations of the Newton–Krylov algorithm presented in Alam (2011). A dynamically adaptive sparse mesh is obtained naturally from the location of significant eddies. The adaptive mesh generation technique is theoretically similar to what was used by Alam (2006) and Alam (2011); the extension in the present work is due to implementation, and hence, is not documented. The algorithm conserves energy, despite the advective form of the nonlinear term that has been employed in (4b), as well as the sparse grid (see Alam 2011). A projection method is applied to solve (4a) and (6a), in which we have adopted a multigrid V-cycle algorithm for solving the corresponding pressure equation (Wesseling 1992).

## 3. Validation of the MES model

In this section, the results delivered by the proposed MES model for the simulation of a turbulent Ekman layer are summarized. A principal objective aims to confirm that the MES model simulates a neutral Ekman boundary layer of a dry atmosphere.

### 3.1. *Reference models for comparison*

We have considered two sets of reference DNS results at $Re = 8000$ for validation of the present model. One is presented by Coleman *et al.* (1990) and the other by Morris *et al.* (2010). The computational domain of Morris *et al.* (2010) is larger than that of Coleman *et al.* (1990), but both results are dynamically equivalent, and agreed well with experimental measurements. In dimensionless coordinates, the computational domain for the present simulation is very close to that of Morris *et al.* (2010).

### 3.2. *Parameters and conditions*

The model domain is $x \times y \times z = 25\,\text{km} \times 10\,\text{km} \times 4\,\text{km}$, where the $f$-plane rotates about the $z$ axis at the rate determined by the Coriolis parameter $f = 10^{-4}\,\text{s}^{-1}$. The flow is driven by a constant pressure gradient in the $y$-direction, where the far-field geostrophic wind is in the $x$-direction. For the purpose of comparison with reference models, we have used a characteristic length scale $L = 4\,\text{km}$ (domain height), a geostrophic wind vector $\boldsymbol{V}_g = \langle G, 0, 0\rangle$ with $G = 4\,\text{m/s}$, and a constant eddy viscosity $\nu = 2\,\text{m}^2/s$. Since both the considered reference models do not provide the dimensional parameters, we have estimated the values of $G$ and $\nu$ using the theory and observational data that was reported by Taylor (1915). The value $\nu = 2\,\text{m}^2/s$ is smaller than the typical value $10 - 12.5\text{m}^2/s$ for a neutral ABL (Garratt 1992, p. 42). With these values, we get a Reynolds number $Re = 8000$, and a Rossby number $Ro = 10$, where $Re = GL/\nu$ and $Ro = G/fL$. Representative parameters are listed in table 1. We have considered $Re$ in the range between 2000 and 18 000.

With this set of parameters, the viscous depth of the Ekman layer, defined by $\delta = \sqrt{2\nu/f}$, is $\delta = 200\text{m}$, which results in an Ekman Reynolds number $Re_{ek} = 400$, and is the same as that of Coleman *et al.* (1990). The dimensionless computational domain is $L_x \times L_y \times L_z = 6.25 \times 2.5 \times 1$, which is about the same ($\approx 2\pi \times 3\pi/4 \times 1$) as that employed in the reference model, e.g. Morris *et al.* (2010). As listed in table 1, the dimensionless Ekman layer depth, $\delta$, is about 5% of the domain height at $Re = 8000$, which is also in agreement with the simulation of Morris *et al.* (2010). Corresponding simulations have an Ekman layer depth $\sim$ 130–285 m. These parameters represent a typical neutrally stratified atmospheric condition.

The lowest numerical resolution at scale $s = 0$ is defined by $(m_x + 1) \times (m_y + 1) \times (m_z + 1)$, and the highest numerical resolution at an arbitrary scale $s$ is $(N_x + 1) \times (N_y + 1) \times (N_z + 1)$, where $N_x = m_x 2^s$, $N_y = m_y 2^s$, and $N_z = m_z 2^s$ are the number of partitions in $x$, $y$ and $z$ directions respectively. We have used $m_x = m_y = m_z = 4$, where all simulations begin with 75 eddies arranged uniformly on a $5 \times 5 \times 5$ grid at the largest scale. The smallest scale of the resolved eddies is given by $\Delta x \sim L_x/N_x$, $\Delta y \sim L_y/N_y$, and $\Delta z \sim L_z/N_z$. When $s = 6$, i.e. after 7 levels of refinement, all eddies will be arranged on the finest grid $257 \times 257 \times 257$ if no filtering is applied. Starting with $\epsilon = 10^{-1}$ and reducing the value each time by a factor of 2, we have found that $\epsilon = 10^{-2}$ results in good agreement with the reference results.

Table 1. Dimensionless parameters for validating the present model. The third column with $Re = 8000$ corresponds to the reference DNS results, and all other columns have been determined equivalently.

| $Re$ | 2000 | 6000 | 8000 | 10 000 | 12 500 | 14 000 | 16 000 | 18 000 |
|---|---|---|---|---|---|---|---|---|
| $Re_{ek}$ | 200 | 346 | 400 | 447 | 500 | 523 | 566 | 600 |
| $L_x$ | $89\delta$ | $108.8\delta$ | $125.6\delta$ | $141\delta$ | $157\delta$ | $166.2\delta$ | $177.7\delta$ | $188.5\delta$ |
| $L_y$ | $33.3\delta$ | $40\delta$ | $47\delta$ | $52.7\delta$ $59\delta$ | $62.3\delta$ | $66.6\delta$ | $76.7\delta$ | |
| $L_z$ | $14\delta$ | $17.3\delta$ | $20\delta$ | $22.4\delta$ $25\delta$ | $26.5\delta$ | $28.3\delta$ | $30\delta$ | |

### 3.2.1. *The initial flow and its evolution to organized eddies*

The exact solution for a laminar Ekman layer flow that has been perturbed with a random velocity field having a prescribed (von Karman-type) energy spectrum

$$E(k) = \frac{g_2 k^4}{\left(g_1 + k^2\right)^{17/6}} \exp\left(-\frac{k^2}{k_{\max}^2}\right),$$

where $g_1 = 0.558$ and $g_2 = 1.196$ are constants (Fung *et al.* 1992). $k_{\max} = 16$ is kept for all simulations. Figure 3 presents the time evolution of the mean kinetic energy (normalized with respect to the initial kinetic energy) for a range of Reynolds numbers. A statistically stationary state of turbulence is found on the basis of time series of the kinetic energy. In the Ekman boundary layer, the pressure gradient force is balanced by the Coriolis force, providing large-scale energy input into the system. The energy of the 3D turbulent flow is transferred from large to small scales by the non-linear inertial force, where the energy is dissipated by the action of SGS effects. This energy transfer is accompanied by the creation of small-scale eddies that are usually intermittent. Figure 3 implies the balancing of the mean shear production of

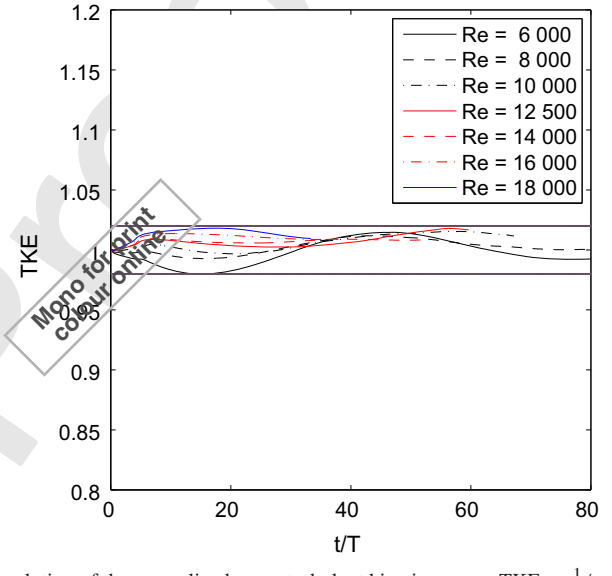


Figure 3. The time evolution of the normalized mean turbulent kinetic energy, TKE $= \frac{1}{2}\langle u_i \rangle_\epsilon^s \langle u_i \rangle_\epsilon^s$, for a range of Reynolds numbers, $6000 \leq Re \leq 18\,000$, with $\epsilon = 10^{-2}$. A statistically stationary turbulence is observed with at most 2% fluctuation in the kinetic energy. Each time series has been normalized with respect to the first data item at $t/T = 0$. The curve identification is best done at near $t/T = 20$, where the curves with line-style identified by the inset correspond values of $Re$ increasing in concert with the value of TKE.

turbulent kinetic energy by the dissipation. The overall production and dissipation differ by about 2% near $t/T = 15$, indicating that the dissipation is dominant for the lowest $Re$, and the production is dominant for the highest $Re$.

### 3.3. *Analysis of the numerical results*

Our goals are to demonstrate that the overall structure of a neutrally stratified atmospheric Ekman boundary is captured by resolving significant eddies, where insignificant eddies are modeled with a multiscale parameterization scheme. Does the MES approach reproduce the known vertical structure of the turbulent Ekman layer in the ABL? Given the complexity and challenges of atmospheric turbulence (Wyngaard 1992), would the MES simulations help explain meteorological observations in the ABL if the model were extended to simulate the ABL in more realistic conditions?

#### 3.3.1. *Model validation*

When the flow has reached a statistically stationary state, a spatial average in the horizontal plane has been taken for computing mean velocities $\langle u\rangle$ and $\langle v\rangle$ as a function of the vertical coordinate, $z/L$. Profiles of $\langle u\rangle$ and $\langle v\rangle$ are presented in figure 4, which shows that a variation in $Re$ leads to a variation in the depth over which the velocity profile changes significantly. At $Re = 8000$, our simulation corresponds to the simulation reported by Coleman *et al.* (1990) at the same value of $Re$ (e.g. the case A45N, $Re_{\mathrm{ek}} = 400$). This correspondence helps to understand the degree to which the present MES simulation resembles an Ekman ABL. The vertical structure of the Ekman layer at $Re = 8000$ – as depicted in figures 4(a),(c) – is approximately the same as what is seen from Fig. 10a of Coleman *et al.* (1990). In light of this qualitative comparison, a fundamental quantitative assessment for a neutrally stratified shear turbulence in the ABL is to estimate the depth of the Ekman layer as a function of $Re$. Data from table 1 show that an increase of $Re$ decreases $\delta$ approximately as $Re^{-1/2}$. More specifically, $\delta/L \approx 4.47 Re^{-1/2}$, which is in agreement with $\delta = \sqrt{2G/f}\,L Re^{-1/2}$. This indicates that the mean boundary layer flow matches the geostrophic wind at a height $\delta$ above the ground.

In Coleman *et al.* (1990), a length scale defined by $D = u^*/f$ is used, where $u^* = \sqrt{\tau/\rho_0}$ is the friction velocity, $\rho_0$ is the reference density, and $\tau$ is the magnitude of the mean shear stress at the bottom boundary, and a value of $\delta = 0.07D$ was reported. With the present set of parameters, we have also checked that the simulated flow at $Re = 8000$ has resulted in $\delta = 0.065D$, which is in good agreement with that of Coleman *et al.* (1990).

As mentioned earlier, the data in table 1 agree with the estimate $\delta \sim Re^{-1/2}$. In figures 4(b),(d), we have zoomed in upon the lowest 200m ($z \leq 0.05L$), and marked this distance with the symbol $\circ$, which is at a distance $\propto Re^{-1/2}$ from a fixed location on the ground. These velocity profiles show that the Ekman layer height decreases with an increase of $Re$. The good agreement of these velocity profiles with the theoretical estimate $\delta \sim Re^{-1/2}$ (Coleman *et al.* 1990, Morris *et al.* 2010) confirms that the MES model has simulated a turbulent Ekman layer in spite of the fact that only a few significant eddies have been resolved (see also table 2). These mean velocity profiles are also in very good agreement with those presented in Coleman *et al.* (1990) (e.g. figure 10a).

The mean velocity $Q^+ = (\sqrt{\langle u\rangle^2 + \langle v\rangle^2})/u^*$ is presented in figure 5($a$) as a function of the normalized vertical coordinate $z^+ = zu^*/\nu$ for $Re = 8000$, 12 500, and 18 000. A good qualitative agreement of $Q^+$ with the logarithmic law of the wall is interesting because the

Table 2. A comparison between the number of eddies captured at various resolutions $129\times129\times129$, $257\times257\times257$, $513\times513\times513$, and $1025\times1025\times1025$ by the MES model and a DNS model. (Rows 1 and 2 are included for clarity, although they contain the same information.)

| Resolution | $129^3$ | $257^3$ | $513^3$ | $1025^3$ |
|---|---|---|---|---|
| $N$ for DNS | 2 146 689 | 16 974 593 | 135 005 697 | 1 076 890 625 |
| $\mathcal{N}$ for MES | 99 483 | 51 796 | 42 941 | 41 131 |
| $\frac{\mathcal{N}}{N}\times100$ | 4.7437% | 0.3087% | 0.0320% | 0.0038% |

present MES model does not employ any near surface parameterization. Given the complexity of the turbulent atmosphere (Wyngaard 1992, Senocak *et al.* 2007), we do not expect that the MES model is sufficient to fully resolve the near surface turbulent structures. However, the demonstration on the law of the wall may encourage further studies with the MES approach. In figure 5(b), the hodograph of the simulated turbulent flow is compared with the laminar Ekman layer solution, which also confirms that the velocity profiles in figure 4 correspond to a turbulent Ekman layer flow. In our simulation, the angles between the direction of the shear stress at wall and that of the geostrophic wind for laminar and turbulent Ekman layer flow are 45° and 28.8°, respectively. Shingai and Kawamura (2004) obtained 28.7° for the turbulent Ekman layer, whereas Morris *et al.* (2010) observed 28.79° for the same. The physical experiment of Caldwell *et al.* (1972) yielded 28°.

Historically, Ekman (1905) investigated the observed drift of ice floes angled at 20–40° to the right of the geostrophic wind direction in the northern hemisphere. Using a constant eddy viscosity model, Ekman's solution predicts a cross-isobaric angle 45°, and did not agree with the observed angle. Independently, Taylor (1915) developed an ABL model with an improved prediction of the cross-isobaric angle. Following these pioneering works, the vertical structure of the Ekman boundary layer of the dry atmosphere is represented by the hodograph and the cross-isobaric angle. In other words, resolving the hodograph, and predicting the direction of the flow correctly suggest that the turbulent Ekman boundary layer has been simulated with the MES model. The data presented in this section demonstrate that the MES model results are in agreement with previously reported results from DNS analyses, experimental observations, and theoretical estimates.

### 3.3.2. *Numerical experiment at the highest resolution*

In the context of LES, the number of resolved eddies may be considered as the number of energetic degrees of freedom $\mathcal{N}$. Increasing the resolution by a factor of 2 in each direction would increase $\mathcal{N}$ by a factor of 8. Due to this scaling, LES prediction of the ABL is severely limited by the computer's power (Beare and Macvean 2004, Sorbjan 2006). We now demonstrate that for a prescribed measure of the strength of significant eddies and the Reynolds number, the number, $\mathcal{N}$, exhibits an asymptotic limit for a given $\epsilon$.

Table 2 presents the number of significant eddies captured by the MES model at four different resolutions: $129\times129\times129$, $257\times257\times257$, $513\times513\times513$, and $1025\times1025\times1025$, and compares the number of DNS eddies $N$ with that of MES eddies $\mathcal{N}$. For the highest resolution, there are only about 41 131 significant eddies that have been resolved at each time step, and $\mathcal{N}\approx0.0038\%N$. Starting with only 75 eddies at the coarsest resolution $5\times5\times5$, we have searched for eddies with a strength $\geq\epsilon$ up to the resolution $2049\times2049\times2049$. In this simulation, all eddies at a resolution that is higher than $1025\times1025\times1025$ are found to have a strength $<\epsilon$, and such eddies are parameterized. The highest resolution has been determined

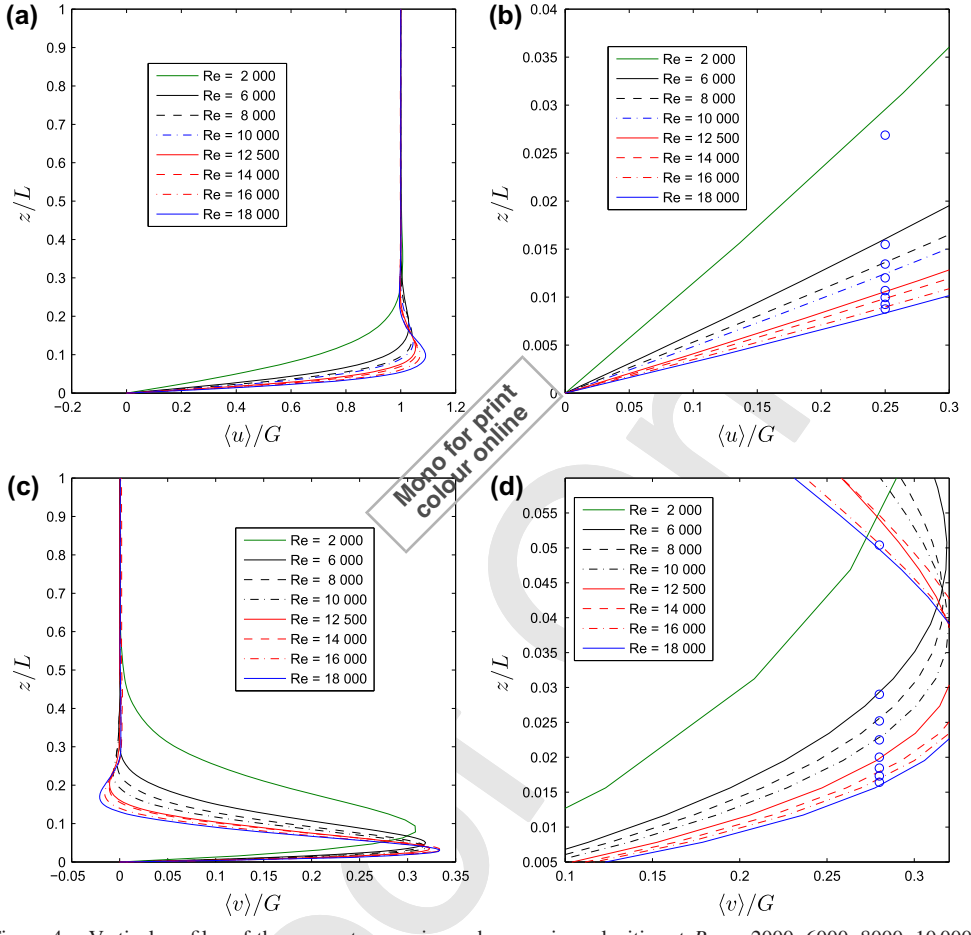


Figure 4. Vertical profiles of the mean stream-wise and span-wise velocities at $Re = 2000, 6000, 8000, 10\,000, 12\,500, 14\,000, 16\,000, 18\,000$: (a) stream-wise velocity, $\langle u\rangle/G$, (b) same as (a), but zoomed in for showing $\delta \sim Re^{-1/2}$ with the symbol ∘, (c) span-wise velocity, $\langle v\rangle/G$, and (d) same as (c), but zoomed in for showing $\delta \sim Re^{-1/2}$ with the symbol ∘. The velocity and the vertical coordinate are normalized with respect to $G(= 4\text{m/s})$ and $L(= 4\text{km})$, respectively. The vertical extent of the boundary decreases as $Re$ increases. So in the "zoomed in" figure (b) the curves with line-style identified by the inset correspond to values of $z/L$ at fixed $\langle u\rangle/G$ that decrease in concert with increasing $Re$.

dynamically based on $\epsilon = 10^{-2}$. Note also that $\mathcal{N} \sim 41\,131$ is about $33 \times 33 \times 33$, which indicates the reduction of computational work in the present MES model.

In order to estimate the efficiency of the algorithm employed for resolving multiscale significant eddies, a scaling between the number of significant eddies and the CPU time has been examined. Here, the CPU time is the elapsed time that is needed to advance the simulation for one time step, and a time series for CPU time is obtained by recording the elapsed time at each time step. For comparison purposes, we have normalized both time series, $\mathcal{N}(t)$ and CPU($t$), with respect to the last data item in each series. The plots in figure 6 show that the growth in the number of eddies at each time step is approximately proportional to the CPU time. Hence, the MES model is fully optimal although significant eddies are identified and less-significant eddies are removed at each time step.

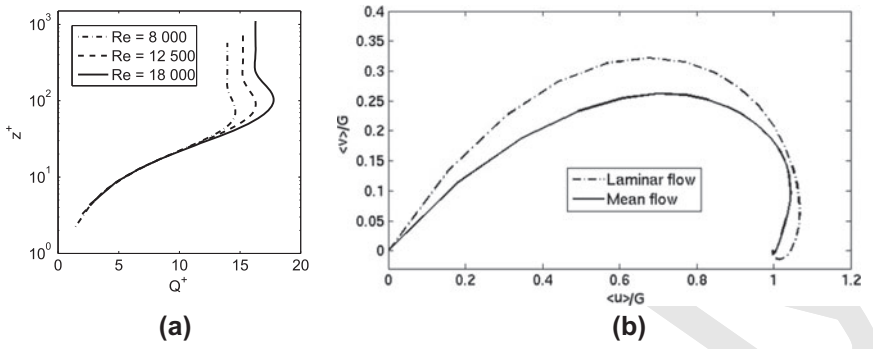


Figure 5. (a) The absolute mean velocity $Q^+ = \left(\sqrt{\langle u\rangle^2 + \langle v\rangle^2}\right)/u^*$ as a function of $z^+$ for $Re = 8000, 12\,500, 18\,000$. (b) The hodograph of mean turbulent velocity $Re = 8000$ has been compared with that of laminar Ekman layer solution.

Each plot in figure 6 indicates a spin-up period of 1 to 1.25 h, during which turbulent kinetic energy cascades through the entire inertial range. After this spin-up period, the Ekman layer turbulence is fully developed and strongly intermittent (Morris *et al.* 2010). In other words, the most energetic turbulent motion is confined in a fraction of the entire domain, and hence, the number of MES grid points ($\mathcal{N}$) has been reduced drastically compared to that ($N$) needed for directly resolving turbulent motion (see table 2). Note also that the abrupt fluctuations in figure 6 are associated with the spatio-temporal intermittency of turbulence.

### 3.3.3. *Intermittent turbulence in the Ekman layer*

In the ABL, the near-surface friction velocity, $u^*$, provides information on the global intermittency (Mahrt 1999), where the law of the wall

$$\frac{U(z)}{u^*} = \frac{\ln z}{\kappa} + C$$

defines the mean horizontal velocity $U(z)$ as a function of the vertical distance from the Earth's surface. Here, $\kappa$ is the von Karman constant and $C$ is an empirical constant. Matching this velocity profile to the edge of the surface layer at $10.7\nu/u_*$ one finds that (Garratt 1992)

$$\frac{U(z)}{u_*} = \frac{\ln(zu_*/\nu)}{\kappa} + 5.0\,.$$

Under neutral conditions, when the viscous sub-layer is deeper than the surface roughness, experimental data (Garratt 1992, Chapter 4) indicate that the aerodynamic roughness length is $z_0 \approx 0.11\nu/u_*$. For example, with $\nu = 2\mathrm{m}^2/s$ and $u_* = 0.3$m/s, we get $z_0 \sim 0.7$ m, which is smaller than minimum $\Delta z$ in our adaptive mesh simulation. These estimates help to replace the law of the wall by $U(z)/u_* = (1/\kappa)\ln(z/z_0)$ (Garratt 1992). We have used $z_0$ that is approximately equal to the smallest $\Delta z$ near the surface, and $\kappa = 0.41$. Clearly, unsteady horizontal fluctuations of the velocity near the surface may lead to fluctuations in the friction velocity $u^*$, and these fluctuations are the signature of the presence of intermittent eddies near the surface. A time series of $u^*$ has been recorded at each time step of the MES simulations, where a dynamically adapted time step, $\Delta t$, between $9 \times 10^{-2}$ and $2 \times 10^{-1}$ is used such that the maximum CFL number does not exceed a value of 4. The time series of $u^*$ has been (block)

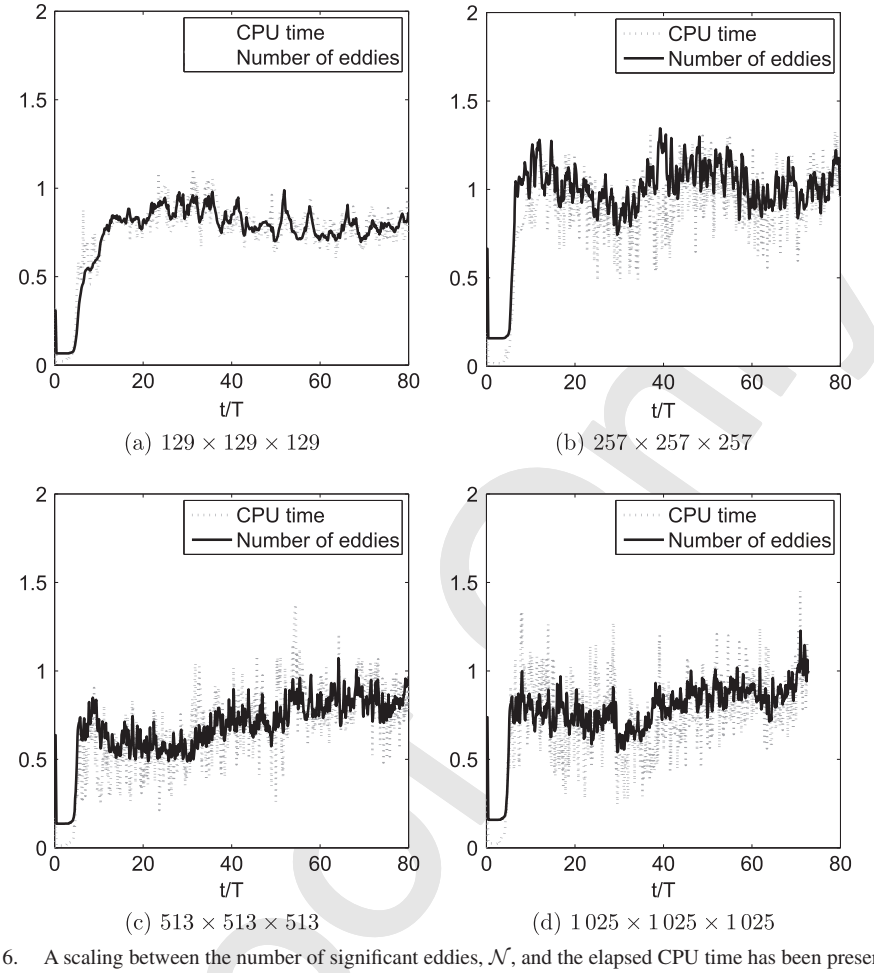


Figure 6. A scaling between the number of significant eddies, $\mathcal{N}$, and the elapsed CPU time has been presented at $Re = 8000$ for various resolutions (e.g. table 2). (a) $129 \times 129 \times 129$, (b) $257 \times 257 \times 257$, (c) $513 \times 513 \times 513$, and (d) $1025 \times 1025 \times 1025$. Each time series in this figure has been normalized with respect to the last data item of the corresponding series. The numbers of significant eddies corresponding to each of the plots are given in table 2.

averaged every 5 time steps, and $u^*/G$ is presented in figure 7 for $3.6 \leq t/T \leq 90$, where $G = 4\text{m/s}$ and $T = 1000\text{s}$. To understand the meaning of a trend in the fluctuations of $u^*$, the data have also been averaged every 50 time steps, and the result is also presented in figure 7. Our numerical simulations indicate that random perturbations of laminar Ekman layer flow develop intermittent fluctuating vortices during the first hour (spin-up time, $t/T = 3.6$). These vortical structures persist as can be seen from the 24-hour period of $u^*$ in figure 7. The mean behaviour of $u^*$ is also in good agreement with that reported for the DNS model of Coleman *et al.* (1990). The time evolution of $u^*$ in figure 7 exhibits global intermittency in the neutrally stratified ABL.

Figure 8 presents the temporal evolution of the vertical vorticity on a horizontal plane at about $z = 39\text{m}$ from the ground for $t = 1.0$, 1.5, and 10 h. During the first hour from the time of model initialization, perturbations to the initial flow have grown, and during this spin-up period most of the eddies are found to be large in size (figure 8(a)). Soon after the spin-up

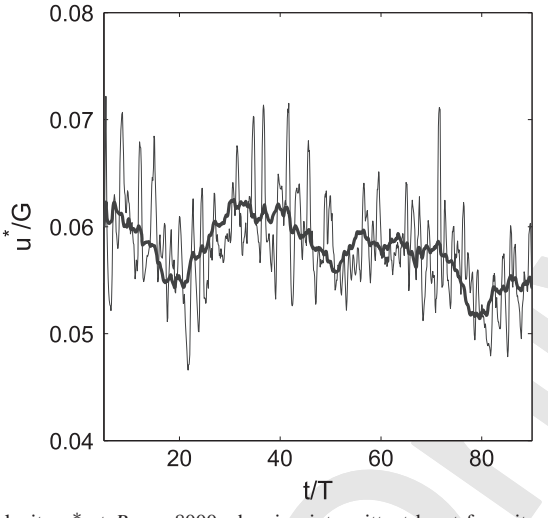


Figure 7. The friction velocity $u^*$ at $Re = 8000$, showing intermittent burst from its mean value 0.065, where $G = 4\text{m/s}$ and $T = 1000\text{s}$. Noticeable fluctuation in the friction velocity has been observed despite the flow being neutrally stratified.

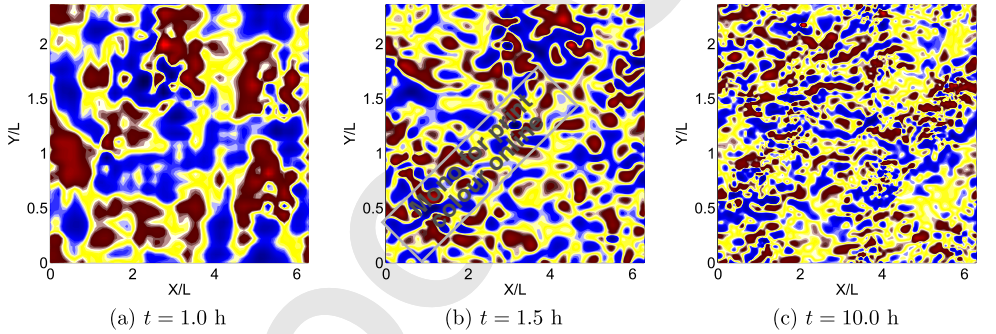


(a) $t = 1.0$ h (b) $t = 1.5$ h (c) $t = 10.0$ h

Figure 8. The vertical vorticity at $z = 39\text{m}$ and $Re = 8000$ after 1.0, 1.5, and 10 h, respectively, from model initialization, where the length scale is $L = 4\text{km}$. The formation of small-scale eddies has been observed as the simulation time elapses.

period ($t = 1.5$ h, figure 8(b)), the flow becomes fully turbulent along with the presence of intermittent eddies, which is depicted in figures 8(b),(c) with the vertical vorticity after 1.5 and 10 h, respectively, from model initialization. The energy cascade appears to be associated with strong intermittency, where the energetic eddies have increased in number and decreased in size, and the intermittency persists (e.g. figure 8(c)), where turbulence is less and less space filling before dissipation takes place (Frisch *et al.* 1978, Kevlahan *et al.* 2007). This intermittency is also evident in figure 6 showing abrupt fluctuations in the number of significant eddies after about 1.25 h.

The formation of intermittent eddies and their vertical updrafts on a vertical $x$-$z$ plane at $y/L = 1.25$ for $Re = 16\,000$ have also been presented in figures 1(a),(b). Noticeable vertical updrafts have been observed under neutral conditions. In particular, the results presented in figures 1, 6, 7, and 8 indicate that a strongly intermittent and turbulent Ekman layer has been simulated under neutral conditions.

## 4. Conclusion, discussion, and future research direction

### 4.1. *Conclusion*

The development of a novel multiscale intermittent eddy simulation methodology – the MES model – for the ABL has been investigated. This MES model simulates an ABL flow at a high resolution $1025 \times 1025 \times 1025$ using about 41 131 significant eddies at $Re = 8000$. Since the number 41 131 is about $33 \times 33 \times 33$, one clearly sees the benefits of the proposed model. We have briefly outlined the MES methodology, showing how a lifting scheme-based wavelet transform approach can be adopted to filter the most significant eddies. We have studied a multiscale approach to parameterize the effect of unresolved eddies.

We have investigated a neutrally stratified turbulent Ekman layer for Reynolds numbers in the range of $2000 \leq Re \leq 18\,000$. The estimated Ekman layer depth, $\delta$, of the simulated flow is on the order of the typically observed scale 130–285m. The neutral Ekman layer is of course only an idealized realization of the ABL. However, our results show that the neutral Ekman layer is highly intermittent at a small scale. In this article, our principal objective is to explore the performance of the MES model for simulating turbulent flows that closely resemble the ABL so that we can advance the MES methodology as a potential research methodology in the field of atmospheric modeling.

As discussed in section 2.1, a number of recent works demonstrated the benefits of the wavelet method in turbulence modelling and simulation. However, little is known about how to extend the wavelet method to the field of atmospheric modelling. This article studies a novel methodology that takes advantage of the promise of wavelets to model turbulence intermittency by filtering large energy-containing eddies scale by scale. As a result, the number of resolved calculations has been reduced drastically with respect to a classical LES (see table 2).

We like to mention two similar developments. de la Llave Plata *et al.* (2012) used the 1-dimensional Burgers' equation to demonstrate the use of bi-orthogonal wavelets for LES, and mainly examined the performance of wavelets to decompose a simulated turbulent flow. On the other hand, Stefano and Vasilyev (2013) employed the second-generation wavelet method to solve the classical LES equations for isotropic turbulence, and studied an explicit wavelet filtering approach for SGS stress. In contrast, the present work introduces a novel methodology to simulate large eddies in the ABL, where the surface-induced drag and the Earth's rotation produce a spiral motion of the mean wind profile. Our knowledge on the near surface prediction of atmospheric eddies has been mainly confined to meteorological observations. Given the geostrophic forcing (e.g. from observation), we have found that a cluster of wavelets behave like atmospheric eddies, which predicts the near surface flow and its direction, i.e. the Ekman spiral with sufficient accuracy (in comparison to observation and reference model). We hope that this work may outline a potential future research direction for the atmospheric modelling research community.

### 4.2. *Future development*

The present article has investigated the potential of the proposed MES model, which suggests a novel research direction for the field of atmospheric modeling. However, further investigation is necessary to explore the full benefits of MES modeling. While the present simulation explains how intermittent eddies can be captured at multiple length scales, simulations of stratified ABL are expected to provide further information concerning the benefits of the MES model.

It may be useful to note that the Ekman boundary layer is an idealization of the ABL. Taylor (1915) demonstrated that the neutral Ekman layer of a dry atmosphere carries significant fundamental properties of the ABL, and helps to develop regional scale weather prediction systems; for example, the secondary circulation associated with the Ekman pumping is responsible for the spin-down of weather systems. Therefore, with respect to the difficulties with ABL turbulence, as well as the very complex nature of the wavelet method, the present work provides a good understanding for potential future extension of the MES modeling approach.

## Acknowledgements

J.M.A. acknowledges the financial support received from the National Science and Engineering Research Council (NSERC) in the form of a Discovery Grant. We also acknowledge computational facilities provided by ACEnet, the regional high performance computing consortium for universities in Atlantic Canada. Suggestions from two anonymous reviewers have improved this article.

## References

Alam, J., A space-time adaptive wavelet method for turbulence. Ph.D. Thesis, Department of Mathematics, McMaster University, 2006.

Alam, J., Towards a multi-scale approach for computational atmospheric modelling. *Mon. Weather Rev.* 2011, **139**, 3906–3922. AQ2

Andrén, A., Brown, A.R., Graf, J., Mason, P.J., Nieuwstadt, F.T.M. and Schumann, U., Large-eddy simulation of a neutrally stratified boundary layer: A comparison of four computer codes. *Q. J. R. Met. Soc.* 1994, **120**, 1457–1484.

Basu, S. and Porté-Agel, F., Large-eddy simulation of stably stratified atmospheric boundary layer turbulence: A scale-dependent dynamic modeling approach. *J. Atmos. Sci.* 2006, **63**, 2074–2091.

Batchelor, G.K. and Townsend, A.A., The nature of turbulent motion at large wave-numbers. *Proc. R. Soc. Lond. A* 1949, **199**, 238–255.

Beare, R. and Macvean, M., Resolution sensitivity and scaling of large-eddy simulations of the stable boundary layer. *Bound.-Lay. Meteorol.* 2004, **112**, 257–281.

Berger, M.J. and Collela, P., Local adaptive mesh refinement for shock hydrodynamics. *J. Comp. Phys.* 1989, **82**, 64–84.

Brasseur, J.G. and Wei, T., Designing large-eddy simulation of the turbulent boundary layer to capture law-of-the-wall scaling. *Phys. Fluids* 2010, **22**, 021303–21. AQ3

Caldwell, D.R., Van Atta, C.W. and Helland, K.N., A laboratory study of the turbulent Ekman layer. *Geophys. Fluid Dyn.* 1972, **3**, 125–348.

Coleman, G.N., Similarity statistics from a direct numerical simulation of the neutrally stratified planetary boundary layer. *J. Atmos. Sci.* 1999, **56**, 891–900.

Coleman, G.N., Ferziger, J.H. and Spalart, P.R., A numerical study of the turbulent Ekman layer. *J. Fluid Mech.* 1990, **213**, 313-348.

Coleman, G.N., Ferziger, J.H. and Spalart, P.R., Direct numerical study of the stably stratified turbulent Ekman layer. *J. Fluid Mech.* 1992, **244**, 677–712.

Coleman, G.N., Ferziger, J.H. and Spalart, P.R., A numerical study of the convective boundary layer. *Bound.-Lay. Meteorol.* 1994, **244**, 247–272.

Costa, F.D., Acevedo, O.C., Mombach, J.C.M. and Degrazia, G.A., A simplified odmel for intermittent turbulence in the nocturnal boundary layer. *J. Atmos. Sci.* 2011, **68**, 1714–1729.

Coulter, R., A case study of turbulence in the stable nocturnal boundary layer. *Bound.-Lay. Meteorol.* 1990, **52**, 75–91.

de la Llave Plata, M. and Cant, R., A wavelet-based multiresolution approach to large-eddy simulation of turbulence. *J. Comp. Phys.* 2010, **229**, 7715–7738.

de la Llave Plata, M., Cant, S. and Prosser, R., On the use of biorthogonal interpolating wavelets for large-eddy simulation of turbulence. *J. Comp. Phys.* 2012, **231**, 6754–6769.

Deardorff, J.W., A three-dimensional numerical investigation of idealized planetary boundary layer. *Geophys. Fluid Dyn.* 1970, **1**, 377–410.

Deardorff, J.W., Numerical investigation of neutral and unstable planetary boundary layer. *J. Atmos. Sci.* 1972, **29**, 91–115.

Domingues, M.O. Jr, Mendes, O. and da Costa, A.M., On wavelet techniques in atmospheric sciences. *Adv. Space Res.* 2005, **35**, 831-842. Fundamentals of Space Environment Science.

Ekman, V.W., On the influence of the earth's rotation on ocean currents. *Ark. Mat. Astron. Fys.* 1905, **2**, 1–52.

Farge, M., Schneider, K. and Kevlahan, N.R., Non-Gaussianity and coherent vortex simulation for two-dimensional turbulence using an adaptive orthogonal wavelet basis. *Phys. Fluids* 1999, **11**, 2187–2201.

Frisch, U., Sulem, P.L. and Nelkin, M., A simple dynamical model of intermittent fully developed turbulence. *J. Fluid Mech.* 1978, **87**, 719–736.

Fung, C.H., Hunt, J.C., Malik, N.A. and Perkins, R.J., Kinematic simulation of homogeneous turbulence by unsteady random Fourier modes. *J. Fluid Mech.* 1992, **236**, 281–318.

AQ4 Garratt, J.R., *The Atmospheric Boundary Layer*, 1992 (Cambridge University Press: Cambridge).

Goldstein, D.A. and Vasilyev, O.V., Stochastic coherent adaptive large eddy simulation method. *Phys. Fluids* 2004, **16**, 2497–2513.

AQ5 Hatlee, S.C. and Wyngaard, J.C., Improved subfilter-scale models from the HATS field data. *J. Atmos. Sci.* 2007, **64**, 1694–1705.

Jablonowski, C., Herzog, M., Penner, J.E., Oehmke, R.C., Stout, Q.F., Leer, B. and Powell, K.G., Block-structured adaptive grids on the sphere: Advection experiments. *Mon. Weather Rev.* 2006, **134**, 3691–3713.

Kevlahan, N.R., Alam, J.M. and Vasilyev, O., Scaling of space-time modes with the Reynolds number in two-dimensional turbulence. *J. Fluid Mech.* 2007, **570**, 217–226.

Mahrt, L., Stratified atmospheric boundary layers. *Bound.-Lay. Meteorol.* 1999, **90**, 375–396.

Mallat, S., *A Wavelet Tour of Signal Processing, Third Edition: The Sparse Way*, 2008 (Academic Press: New York).

Marlatt, S., Waggy, S. and Biringen, S., Direct numerical simulation of the turbulent Ekman layer: Evaluation of closure models. *J. Atmos. Sci.* 2012, **69**, 1106–1117.

Mason, P.J. and Thomson, D.J., Large eddy simulations of the neutral-static-stability planetary boundary layer. *Q. J. R. Met. Soc.* 1987, **113**, 413–443.

Miyashita, K., Iwamoto, K. and Kawamura, H., Direct numerical simulation of the neutrally stratified turbulent Ekman boundary layer. *J. Earth Simul.* 2006, **6**, 3–15.

Moeng, C., A large eddy simulations model for of the study of planetary boundary layer turbulence. *J. Atmos. Sci.* 1984, **41**, 2052–2062.

Morris, K., Handler, R.A. and Rouson, D.W.I., Intermittency in the turbulent Ekman layer. *J. Turbul.* 2010, **12**, 1–25.

Nai-Ping, L., Neff, W.D. and Kaimal, J.C., Wave and turbulence structure in a disturbed nocturnal inversion. *Bound.-Lay. Meteorol.* 1983, **26**, 141–155.

AQ6 Nordbo, A. and Katul, G., A wavelet-based correction method for eddy-covariance high-frequency losses in scalar concentration measurements. *Bound.-Lay. Meteorol.* 2013, **146**, 81–102.

AQ7 Pielke, R.A., *Mesoscale Meteorological Modeling*, 2nd ed., 2002 (Academic Press: San Diego).

Schneider, K. and Vasilyev, O.V., Wavelet methods in computational fluid dynamics. *Annu. Rev. Fluid Mech.* 2010, **42**, 473–503.

Schubert, J.F., Acoustic detection of momentum transfer during the abrupt transition from a laminar to a turbulent atmospheric boundary layer. *J. Appl. Meteorol.* 1977, **16**, 1292–1297.

Scott, B.W., Marlatt, S.W. and Sedat, B., Direct numerical simulation of the turbulent Ekman Layer: Turbulent energy budgets. *J. Thermophys. Heat Tr.* 2010, **24**, 544–555.

Senocak, I., Ackerman, A., Kirkpatrick, M., Stevens, D. and Mansour, N., Study of near-surface models for large-eddy simulations of a neutrally stratified atmospheric boundary layer. *Bound.-Lay. Meteorol.* 2007, **124**, 405–424.

Shingai, K. and Kawamura, H., A study of turbulence structure and large-scale motion in the Ekman layer through direct numerical simulations. *J. Turbul.* 2004, **5**, 1–18.

Skamarock, W.C., Klemp, J.B., Duda, M.G., Fowler, L.D., Park, S.H. and Ringler, T.D., A multiscale nonhydrostatic atmospheric model using centroidal voronoi tesselations and C-grid staggering. *Mon. Weather Rev.* 2012, **140**, 3090–3105.

Skamarock, W., Oliger, J. and Street, R.L., Adaptive grid refinement for numerical weather prediction. *J. Comp. Phys.* 1989, **80**, 27–60.

Smagorinsky, J., General circulation experiments with the primitive equations. *Mon. Weather Rev.* 1963, **91**, 99.

Sorbjan, Z., Local structure of turbulence in stably stratified boundary layers. *J. Atmos. Sci.* 2006, **63**, 1526–1537.

Stefano, G.D. and Vasilyev, O.V., Wavelet-based adaptive large-eddy simulation with explicit filtering. *J. Comp. Phys.* 2013, **238**, 240–254.

Sullivan, P.P. and Patton, E.G., The effect of mesh resolution on convective boundary layer statistics and structures generated by large-eddy simulation. *J. Atmos. Sci.* 2011, **68**, 2395–2415.

Sweldens, W., The lifting scheme: A construction of second generation wavelets. *SIAM J. Math. Anal.* 1997, **29**, 511–546.

Taylor, G.I., Eddy motion in the atmosphere. *Phil. Trans. R. Soc. Lond. A* 1915, **215**, 1–26.

Townsend, A.A., Local isotropy in the turbulent wake of a cylinder. *Aust. J. Sci. Res. A* 1948, **1**, 161.

Vindel, J. and Yagüe, C., Intermittency of turbulence in the atmospheric boundary layer: Scaling exponents and stratification influence. *Bound.-Lay. Meteorol.* 2011, **140**, 73–85.

Wesseling, P., *An Introduction to Multigrid Methods*, 1992 (John Wiley & Sons: Chichester).

Wyngaard, J.C., Atmospheric turbulence. *Annu. Rev. Fluid Mech.* 1992, **24**, 205–234.
Zhou, B. and Chow, F.K., Large-eddy simulation of the stable boundary layer with explicit filtering and reconstruction turbulence modeling. *J. Atmos. Sci.* 2011, **68**, 2142–2155.
Zhou, B. and Chow, F., Turbulence modeling for the stable atmospheric boundary layer and implications for wind energy. *Flow Turbul. Combust.* 2012, **88**, 255–277.